FATIGUE PERFORMANCE OF POWER TRANSMISSION TOWER SYSTEM BASED ON WIND VIBRATION FATIGUE

Zhengfa Li,* Jianwei Zhang,* Haining Wang,* and Yijun Bao*

Abstract

High-voltage transmission tower line system is very prone to wind vibration fatigue damage and extreme cases of dynamic collapse damage, so to solve the vibration of the transmission tower line system caused by wind load, the study by building a finite element model to analyse the wind load and wind vibration response, and experimental analysis of the fatigue life of the transmission tower line system and the mechanical properties of the transmission tower under the broken line condition. According to the findings, the pulsating wind speed is within the value range of -20m/s to 20m/s in 200 s, with an overall trend of constant fluctuation, while the displacement, velocity and acceleration response of the five nodes of the transmission tower under the simulated wind load all show the characteristics of small at the bottom and large at the top. In addition, the actual fatigue life of the transmission tower is 50.3 years when the survival rate is 90%, and 21.1 years when the survival rate is 99.9%. Meanwhile, the maximum values of two indicators, maximum displacement at the top and stress value at the stress maximum, appear in the case of working condition 5, which are 2.78 times and 3.43 times of the unbroken case. Taken together, to avoid the damage of transmission lines caused by wind vibration fatigue, the design safety factor of conductors and ground wires should be increased as much as possible, which is of great significance for solving the actual fatigue damage of transmission tower line system under the effect of wind vibration fatigue.

Key Words

Wind vibration response; transmission tower line system; fatigue performance; wind load

1. Introduction

The power industry has gradually become a pillar industry of a country with the development of technology, but with the continuous increase in the quality and quantity of transmission lines, the actual load of transmission

* Division of Construction, State Grid Gansu Electric Power Corporation, Lanzhou 730000, China; e-mail: lizhengfa0228@163.com; zhajwei@126.com; {wangh_ning, bao15693106683}@163.com Corresponding author: Zhengfa Li

towers (TT) is also gradually increasing [1], [2]. From the current frequent power system accidents, the TT line system (TTLS) is highly susceptible to serious damage under the threat of natural disasters, such as typhoons, resulting in the paralysis of the entire power grid and power system [3], [4]. Due to the unique geographical location of transmission lines, secondary disasters caused by collapse of TTs can also bring huge losses to society. The current design method for TT and line systems is difficult to cope with the actual damage caused by natural disasters, and when designing TTs and lines, only materials and other aspects are used to improve their stiffness. Therefore, the study analysed the wind load and wind vibration response (WVR) by constructing a finite element model, and analysed the fatigue life of the TT and the mechanical performance of the TT under disconnection conditions. Its purpose is to effectively reduce the occurrence of vibration problems in the TTLS caused by wind load, and to lay a theoretical foundation for the development of subsequent vibration reduction measures.

The research is mainly conducted from four parts. The first part is a discussion and summary of the relevant research of the current TTLS. The second part mainly analyses the fatigue performance of the TTLS under wind-induced fatigue damage, including the analysis of its wind load characteristics, wind-induced vibration response, and fatigue life. The third part is a study on the fatigue life and mechanical properties of the TTLS under WVR. The final part is a summary and discussion of the entire article.

2. Related Work

High-voltage TT system structure characteristics is very vulnerable to earthquakes, typhoons and other natural disasters, resulting in damage to the tower system structure and even collapse, resulting in a series of serious consequences [5], [6]. In typhoon-prone coastal areas, the WVR of transmission lines is more significant when they are subjected to wind loads. A wide range of domestic and foreign scholars have conducted in-depth research on it. Asyraf *et al.* [7] proposed filament-wound polymer composites as structural constituent materials

for TT cross-arms for the problem of high risk of TTLS in extreme weather, thus providing data support for the stability of TTLS based on verifying its potential application. Bennett J A *et al.* addressed the safety issues of transmission towers during hurricane weather by constructing an energy system optimization model that incorporates hurricane risk, thereby effectively enhancing the response capacity to extreme weather events [8]. İşleyen *et al.* [9] proposed the idea of carbon fibre-reinforced polymer application in transmission lines for the application of wood structural materials in TTLS, thus effectively enhancing the stiffness of the TTLS. Zhao *et al.* [10] addressed the problems related to the vibration performance of TTLS by using tuned mass dampers to influence the vibration response of TTs, thus effectively improving the vibration damping performance of the TTLS.

In addition, Nguyen and Vu [11] designed a classification model depending on integrated differential evolution and optimisation algorithm for the quality problem of TT structure, thus effectively optimising the structural material of TT. Ogbonna V E *et al.* proposed the use of glass fiber reinforced epoxy resin composite materials as insulation materials for transmission towers in response to the stiffness issue of transmission towers in high-voltage transmission lines, effectively enhancing the corrosion and fracture resistance performance of the transmission tower line system [12]. Tapia-Hernández and De-León-Escobedo [13] address the WVR of high-voltage TTs under wind loads by proposing a vulnerability function for the transverse load pattern based on an example of a section of line in Mexico, thus providing data to support the stiffness and strength enhancement of TTs. Qiu *et al.* [14] address the problem of transmission line and the problem of bird hazards in the tower system, by combining lightweight convolutional neural networks based on the proposed method of fault detection in the TTLS, thus effectively improving the safety of transmission lines.

From the research of foreign scholars, it can be seen that the current and related design codes design the TTLS only from the material and structure to strengthen the TTLS stiffness and strength, but the actual natural disasters have strong uncertainty, so the traditional TTLS in the face of the current natural disasters has been difficult to apply. Therefore, the study analyses the wind load and WVR by constructing a finite element model, and actually analyses the fatigue life of the TTLS and the mechanical performance of the TT under the disconnection condition, which can provide new ideas for the TTLS and also provide data and theoretical support for the subsequent research of the vibration damping system, which is innovative.

3. Fatigue Performance Analysis of TT System under Wind Vibration Fatigue Damage

Unlike other tower structures, the head of the TT has a large mass and complex structure, resulting in a more sensitive response to wind vibration. This section first analyses the characteristics of wind load, then studies its WVR, and then analyses the fatigue life of the TTLS.

3.1 Wind Load Characteristic Analysis for TTLS

To address the problems related to the vibration of the TTLS, the fatigue performance of the TTLS was studied under its wind load simulation. The wind loads in practice can be divided into long-period and short-period, with the former usually referred to as mean wind and the latter as pulsating wind [15]. In addition, the parameters related to energy and spatial features can effectively describe the statistical characteristics of fluctuating winds, while the parameters related to energy features include turbulence and the actual power spectrum of fluctuating winds, while the parameters related to spatial features include the integral scale of turbulence and spatial correlation [16]. In wind load simulation, the time history curve obtained from its random process is usually simulated. Currently, research methods for wind load mainly include linear filtering method and harmonic synthesis method [17]. Among them, in specific nodes of actual TT structures, the relevant wind speed can be regarded as a stationary Gaussian randomisation process. Therefore, the harmonic synthesis method can be chosen for simulation, and the actual sampling function of the stationary Gaussian randomisation process can be approximated using trigonometric function simulation, as expressed in equation (1).

$$x^d(t) = \phi_x^2 \sqrt{\frac{2}{\varphi}} \sum_{i=1}^{\varphi} \cos(s_i t + \delta_i) \qquad (1)$$

In (1), $x^d(t)$ denotes the approximate simulated value of the sampling function of the smooth Gaussian stochastic process $x(t)$; ϕ_x^2 denotes the variance; s_i denotes the randomness variable of the density function of the correlation probability; δ_i denotes the randomness variable with values from 0 to 2π; φ denotes a positive integer that tends to infinity continuously. Among them, the expressions of pulsating WS and pulsating wind force calculation in the simulated form are shown in (2).

$$\begin{cases} M_j(t) = \sum_{i=1}^{j} \sum_{l=1}^{N} |X_{ji}(s_l)| \cdot \sqrt{2\Delta s} \cdot \cos[s_l t - \rho_{ji}(s_l) + \lambda_{il}(s_l)] \\ L_D(t) = \frac{1}{2}\tau Y O_D(\varepsilon)[U(t)]^2 \end{cases} \qquad (2)$$

In (2), $M_j(t)$ represents the pulsating WS in the simulated form; $X_{ji}(s_l)$ represents the value of the elements in row j and column i of the lower triangular matrix at $s = s_l$; $\rho_{ji}(s_l)$ represents the actual phase angle between different loads; λ_{il} represents the randomness value between 0 and 2π; N stands for the actual quantity of samples; $L_D(t)$ represents the pulsating wind; τ represents the actual density of air; Y represents the actual area of the windward side in the effective case of the structure; $O_D(\varepsilon)$ represents the associated drag coefficient corresponding to the angle of attack; and $U(t)$ denotes the time range of WS.

3.2 TTLS Wind Vibration Response Study

Based on the analysis and simulation of wind load characteristics, the WVR of the TTLS is analysed using the time domain. The time-domain method adopts the time-domain method of wind load, which can more accurately obtain the response of the structure under wind load. Therefore, the time-domain method is selected for WVR analysis in the study [18]. Applying Newmark in practical time-domain methods- β) To conduct analysis. The dynamic calculation expression of the TT line structure is shown in (3).

$$W\ddot{p}_{t+\Delta t} + B\dot{p}_{t+\Delta t} + Gp_{t+\Delta t} = Q_{t+\Delta t} + \vartheta_{t+\Delta t} \quad (3)$$

In (3), W represents the mass matrix of the TTLS; $\ddot{p}_{t+\Delta t}$, $\dot{p}_{t+\Delta t}$, and $p_{t+\Delta t}$ represent the acceleration vector, velocity vector, and displacement vector of the nodes; B represents the damping matrix; G represents the stiffness matrix of the TTLS; Q represents the wind spectrum density matrix; ϑ represents the dynamic load array of the nodes; and $t + \Delta t$ represents the time point. Therefore, the differential form of velocity and displacement at $t + \Delta t$ is expressed as shown in (4).

$$\begin{cases} \dot{p}_{t+\Delta t} = \dot{p}_{t+\Delta t} + [(1-\chi)\ddot{p}_t + \chi\ddot{p}_{t+\Delta t}]\Delta t \\ p_{t+\Delta t} = p_t + \dot{p}_t\Delta t + [(\frac{1}{2}-\alpha)\ddot{p}_t + \alpha\ddot{p}_{t+\Delta t}]\Delta t^2 \end{cases} \quad (4)$$

In (4), χ and α denote the quantity of parameters; Δt denotes the time step. The acceleration and velocity at the moment of $t + \Delta t$ are rewritten accordingly to obtain the displacement function expression as shown in (5).

$$\begin{cases} \dot{p}_{t+\Delta t} = \frac{p_{t+\Delta t}}{\alpha\Delta t^2} - \frac{p_t}{\alpha\Delta t^2} - \frac{\dot{p}_t}{\alpha\Delta t} - \frac{(\frac{1}{2}-\alpha)\ddot{p}_t}{\alpha} \\ \dot{p}_{t+\Delta t} = \frac{\chi p_{t+\Delta t}}{\alpha\Delta t} - \frac{\chi p_t}{\alpha\Delta t} + (1-\frac{\chi}{\alpha})\dot{p}_t + \Delta t(1-\frac{\chi}{2\alpha})\ddot{p}_t \end{cases} \quad (5)$$

The optimisation expression obtained by substituting (5) into (3) is shown in (6).

$$G^*p_{t+\Delta t} = E^* \quad (6)$$

In (6), G^* denotes the equivalent stiffness matrix; E^* denotes the dynamic value. The calculated expressions of the corresponding elements in (6) are shown in (7).

$$\begin{cases} G^* = \frac{1}{\alpha\Delta t^2}W + \frac{\chi}{\alpha\Delta t}B + G \\ E^* = Q_{t+\Delta t} + \vartheta_{t+\Delta t} + W\left[\frac{p_t}{\alpha\Delta t^2} + \frac{\dot{p}_t}{\alpha\Delta t^2} + (\frac{1}{2\alpha}-1)\ddot{p}_t\right] + \\ \quad B\left[\frac{\chi p_t}{\alpha\Delta t} - (1-\frac{\chi}{\alpha})p_t - (1-\frac{\chi}{2\alpha})\Delta t\ddot{p}_t\right] \end{cases} \quad (7)$$

When considering the damping calculation of practical engineering, Rayleigh damping assumption is generally chosen, and the corresponding expression is shown in (8).

$$B = \zeta W + \xi G \quad (8)$$

In (8), ξ and ξ represent two constants to be determined. Based on this, the structural damping example
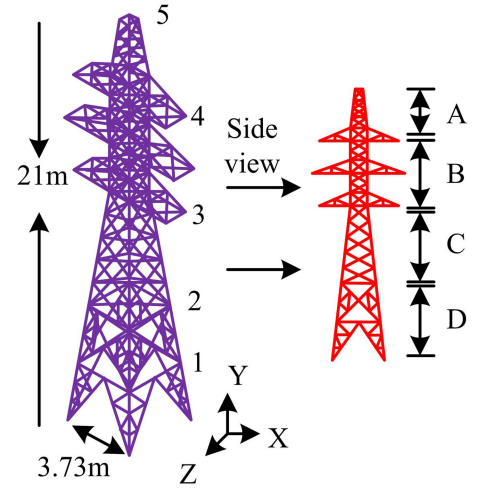
Figure 1. The finite element model structure of the TT.

is shown in (9).

$$\begin{cases} \eta_n = \frac{\zeta}{2s_n} + \frac{\xi s_n}{2} \\ \begin{Bmatrix} \zeta \\ \xi \end{Bmatrix} = \frac{2s_n s_m}{s_n^2 - s_m^2} \begin{bmatrix} s_n & -s_m \\ \frac{-1}{s_n} & \frac{1}{s_m} \end{bmatrix} \begin{Bmatrix} \eta_m \\ \eta_n \end{Bmatrix} \end{cases} \quad (9)$$

In (9), η denotes the structural damping ratio. Therefore, before proceeding to the subsequent fatigue life and mechanical properties of the TTLS, the study constructed a finite element model of an actual TT of 220 kV in finite element analysis software (ANSYS15.0) using hybrid beam-pole cells, and its structure is drawn as shown in Fig. 1.

From Fig. 1, the constructed finite element model of the TT has an overall height of 21 m and a root opening of 3.73 m, which is a typical dry-shaped TT. Due to the actual WS being affected by the vertical height of the TT, the wind load borne by the TT at different height points is different. In order to simplify the actual calculation, the TT contains four sections, set as A–D; and set 5 typical nodes, numbered 1–5.

3.3 Fatigue Life Analysis of Power TT System

Under the action of WVR, the relevant structural components of the TT may experience fatigue damage. Long-term operation of the TT under natural loads such as wind load can lead to accidents such as waist breakage. Therefore, it is necessary to analyse its fatigue life. The actual materials related to TTs and lines have different fatigue limits under different cyclic characteristics. Generally, they can be converted into equivalent zero mean stress. Through comparison, the average stress correction equation (Goodman) was selected for conversion, and the expression of the equation is shown in (10).

$$A_a = A_{-1}\left[1 - \left(\frac{A_m}{A_h}\right)^2\right] \quad (10)$$

In (10), A_a represents the equivalent zero-mean stress; A_{-1} represents the actual strength limit of the material in question; A_m represents the magnitude of the stress; and A_h represents the mean value of the stress. Based on (10), the general expression of the Probability Stress Number of Cycles (P-S-N) curve for lifespan is shown in (11).

$$\lg \tau_q = d_q + c_q \lg A \tag{11}$$

In (11), τ_q represents the fatigue life when the survival probability is q; d_q and c_q represent the material constants associated with the survival probability. When the actual load produces a relevant stress on the material higher than the fatigue limit of the material, each cycle will cause damage to the material, and the accumulated damage is expressed as shown in (12).

$$J = \sum_{r=1}^{\phi} e_r \int E'_r \tag{12}$$

In (12), J indicates the cumulative damage value; e_r indicates the actual number of cycles of the r level load; E'_r indicates the actual fatigue damage under the r level load; ϕ indicates the actual number of levels of variable amplitude load stress level. In the current domestic theory of fatigue damage research, the more widely used assumption is that fatigue damage will occur when the actual energy absorbed by the structure reaches the limit value, based on the assumption of the limit value of the relevant expression is shown in (13).

$$\frac{M'_1}{M'} = \frac{e_1}{E'} \tag{13}$$

In (13), M' indicates the limit value of absorbable energy; E' indicates the total number of cycles. Based on this, the damage rate, fatigue life and total fatigue life are expressed as shown in (14).

$$\begin{cases} SS = \frac{e}{E'} \\ PL = \frac{1}{SS} \\ PL_{\text{Total}} = PL \times t' \end{cases} \tag{14}$$

In (14), SS indicates the damage rate; PL indicates the fatigue life, *i.e.*, the tower will be fatigued after loading PL times; PL_{Total} indicates the total life of the tower; t' indicates the duration of the load.

4. Research on Fatigue Life and Mechanical Properties of TT System under WVR

To verify the fatigue performance of the TTLS, the study first uses numerical simulation to simulate the wind load and use it to derive the WVR, and on the basis of which the fatigue life under wind load is calculated, and finally the mechanical properties such as displacement and stress of the TT under the case of broken line are analysed. Among them, the pulsating WS at a height of 10 m and the synthetic WS correlation curve are shown in Fig. 2.

From Fig. 3, it can be seen that the fluctuating wind speed is within the numerical range of −20 m/s to 20
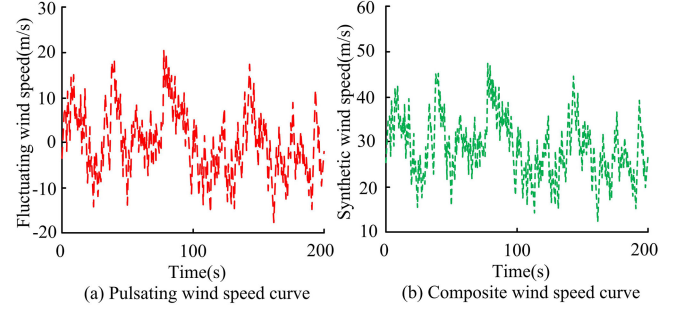
Figure 2. Fluctuating WS curve and composite WS power spectral density curve at 10 m height.
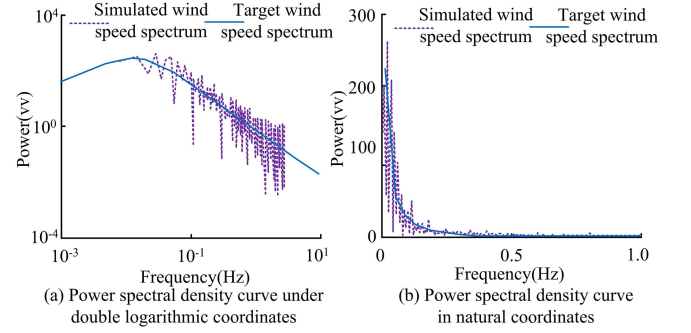
Figure 3. Comparison results of simulated wind speed spectrum and self-power spectral density curve.
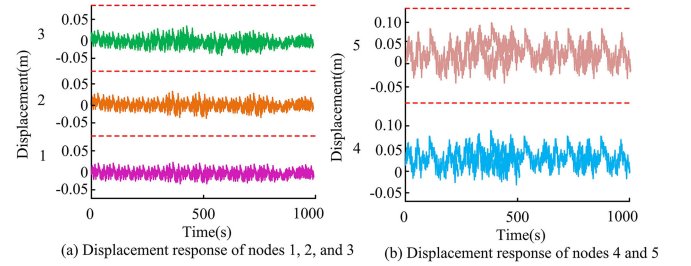
Figure 4. Displacement response results of five typical nodes on the TT.

m/s within 200 s; the synthetic wind speed is within the numerical range of 10 m/s to 50 m/s within 200 s. Therefore, the comparison results of the simulated wind speed spectrum and the self-power spectral density curve based on the wind speed curve results of the two are shown in Fig. 3.

From Fig. 4, under the dual logarithmic coordinate system, the simulated wind speed spectral power fluctuates continuously, and the target wind speed spectral power shows a trend of first increasing and then decreasing. The simulated wind speed spectral power shows a fluctuating and decreasing trend in natural coordinates. Overall, the overall overlap between the two curves is relatively high, indicating the effectiveness of the harmonic synthesis method in simulating wind loads. Among them, the displacement response results of the five nodes in Fig. 1 are shown in Fig. 4.

4

(a) Acceleration response of nodes 1 and 2

(b) Acceleration response of nodes 3

(c) Acceleration response of nodes 4 and 5
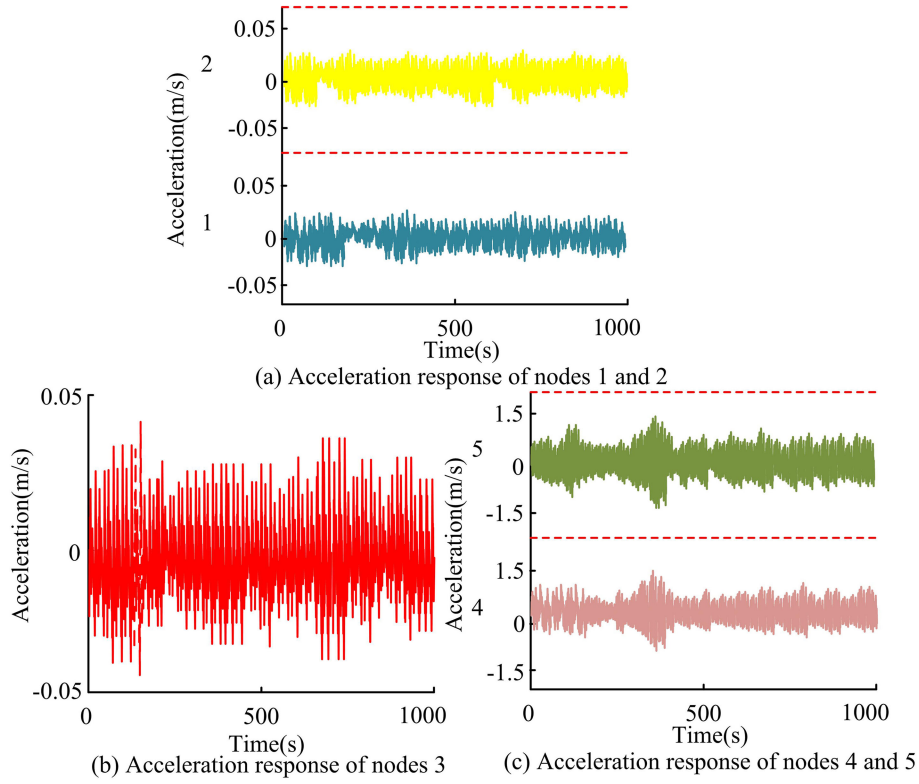
Figure 5. Result of acceleration response of five nodes.

Table 1
Wind-induced WVR and Maximum Displacement Wind-induced Vibration Coefficient of TTs

		Node number				
		1	2	3	4	5
Synthetic WS conditions	Maximum speed	3.046×10^{-1} m/s	2.401×10^{-1} m/s	2.360×10^{-1} m/s	3.357×10^{-1} m/s	11.528×10^{-1} m/s
	Maximum displacement	3.282×10 m^{-2}	2.635×10 m^{-2}	3.632×10 m^{-2}	7.982×10 m^{-2}	8.834×10 m^{-2}
	Maximum acceleration	4.117×10^{-1} m/s^2	4.404×10^{-1} m/s^2	4.692×10^{-1} m/s^2	11.011×10^{-1} m/s^2	10.146×10^{-1} m/s^2
Maximum displacement wind vibration coefficient		2.557	2.603	2.626	2.588	2.659
Static displacement at average WS		1.283×10 m^{-2}	1.012×10 m^{-2}	1.383×10 m^{-2}	3.084×10 m^{-2}	3.322×10 m^{-2}

Comprehensive Fig. 4 illustrated that the displacement response of the five nodes shows an overall trend of fluctuation and fluctuation within 1,000 s. In addition, the results of the acceleration response of the five nodes are shown in Fig. 6.

The combined Fig. 5 shows that the acceleration response of the five nodes fluctuates more frequently within 1000 s. Based on this, the TT WVR and maximum displacement wind vibration coefficients are illustrated in Table 1.

From Table 1, all five nodes show a growing trend in these five indicators, only the maximum acceleration of 10.146 × 10 m/s^{-12} at node 5 is smaller than

that of 11.011 × 10^{-1} m/s^2 at node 4. Comprehensive Figs. 4 and 5 and Table 1, the displacement, velocity and acceleration response of the TT all exhibit the characteristics of small at the bottom and large at the top. On this basis, the rainfall counting method and the P-S-N curve are introduced to calculate the fatigue life of the TT under the wind load. Among them, under the application of rain flow counting method, the nodes of TT in ANSYS15.0 software are analysed for stress. As a result, the stress response and rain flow counting of this node under the wind load of Fig. 4 to Table 1 are shown in Fig. 6.

From Fig. 6, it can be seen that in the stress response curve of the node at the point of maximum stress, the stress

(a) Stress response curve of nodes at the point of maximum stress

(b) Rain flow counting results of node stress response at the point of maximum stress
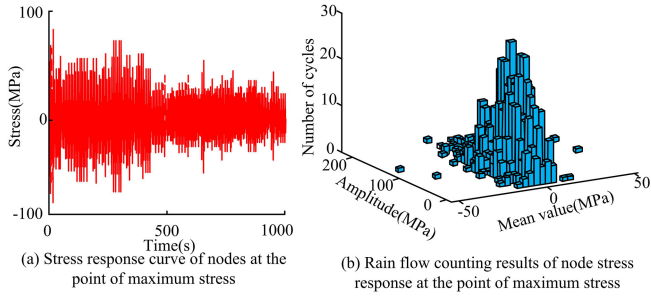
Figure 6. Node stress response and rain flow count at the point of maximum stress at the waist: (a) stress response curves of nodes at the point of maximum stress; and (b) rain flow counting results of node stress response at the point of maximum stress.

value within 1,000 s is similar to the WVR in Figs. 5 and 6, showing a continuous fluctuation trend. Overall, the overall counting results indicate the presence of asymmetric cycles, so (11) can be used to convert to equivalent zero mean stress, and combined with (12) to calculate subsequent fatigue life values. Therefore, the material constant values and survival rates of the TT P-S-N under the action of P-S-N for 90% and 99.9% conditions double logarithmic coordinate system are shown in Fig. 7.

From Fig. 7, with the survival rates of 90% and 99%, the stress values continue to decrease as the number of cycles increases, but the latter has a higher rate than the

(a) The d_q and c_q values of the P-S-N curve of the transmission tower

(b) S-N curves under dual logarithmic coordinates of different survival rates
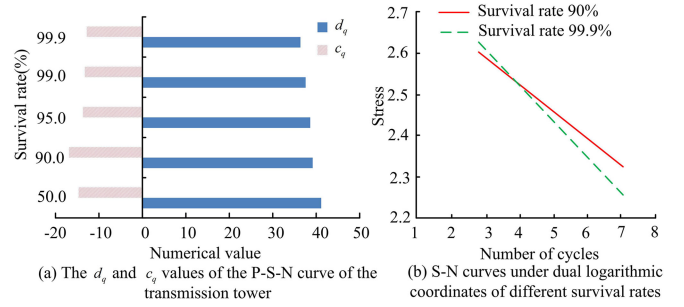
Figure 7. Material constant values and S-N curves for TT P-S-N curves under 90% and 99.9% survival rates:

former. Finally, the wind load simulation method based on Fig. 2 to Fig. 3 is used to simulate the broken line working condition under a 12-step typhoon. The specific breaking conditions include breaking any wire but the ground wire is not broken, breaking any ground wire but the wire is not broken, breaking a wire on each side in the same file, breaking a ground wire on each side in the same file, breaking the wire and ground wire in the same file, and breaking the wire and ground wire on opposite sides in different files. And the six working conditions are set to 1–6, the first two working conditions are asymmetric load, the middle three are symmetric load, and the last working condition is torque load. Among them, the composite wind speed at 10 m below the 12 level typhoon always fluctuates between 0 and 80 m/s, with a

(a) Displacement response results under unbroken working conditions

(b) Displacement response results for condition 1 and condition 2

(c) Displacement response results for condition 3 and condition 4

(d) Displacement response results for condition 5 and condition 6
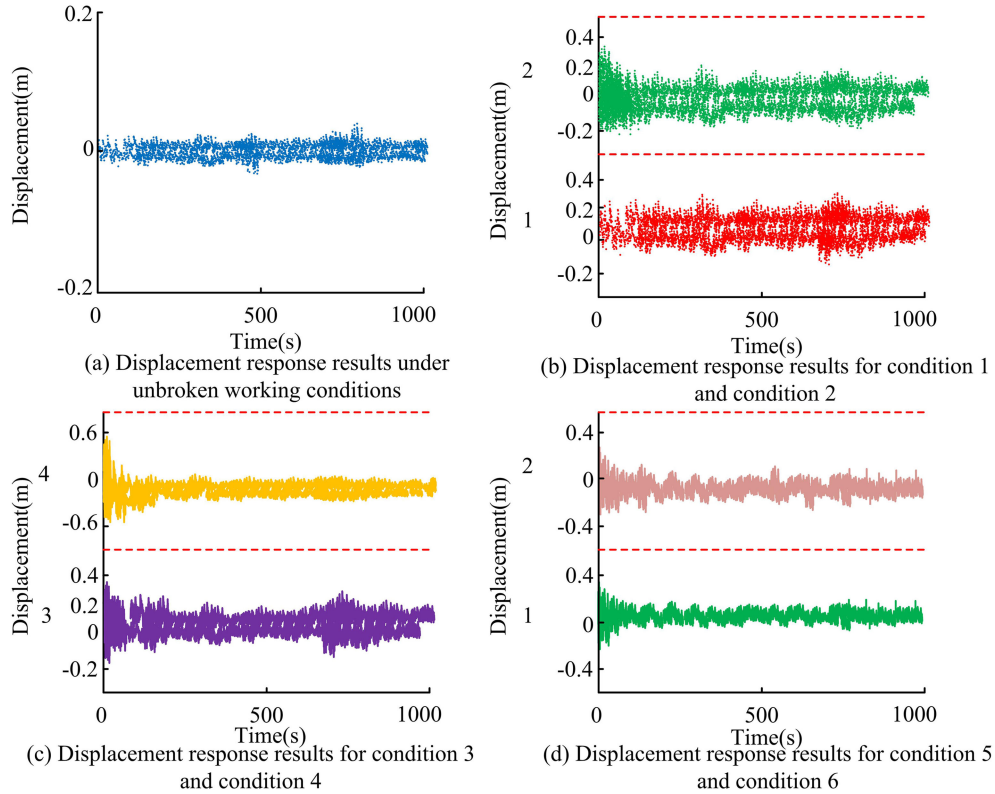
Figure 8. Maximum displacement change at the top under the condition of no disconnection and 6 working conditions: (a) Displacement response results under unbroken working conditions; (b) Displacement response results for condition 1 and condition 2; (c) Displacement response results for condition 3 and condition 4; and (d) Displacement response results for condition 5 and condition 6.

maximum value of about 78 m/s and a minimum value of about 8 m/s. Under this wind speed variation, the average wind speed of 35 m/s was taken for subsequent experiments. Based on this, the maximum displacement changes at the top under the non-disconnection condition and 6 working conditions are shown in Fig. 8.

In Fig. 8, the maximum displacement change within 1,000 s in the unbroken condition is maintained between -0.2 m and 0.2 m, and the difference between the unbroken condition and the condition 1 is not large, but exceeds 0.2 m only in the first few tens of seconds; in the condition 2, the first few tens of seconds are higher than 0.2 m and lower than 0.2 m, and the rest of the interval changes are similar. And the fluctuation change of working condition 4 is the biggest, and the displacement change is between -0.4 and 0.6 in the first few tens of seconds.

5. Conclusion

For the wind load, especially typhoon-induced vibration of high-voltage TTLS, the study constructed a real TT finite element model, and used it to experimentally analyse the WVR of the TTLS, the fatigue life of the TT under wind load and the mechanical properties of the TT under disconnection conditions. According to the findings, the simulated WS spectrum power fluctuates continuously in double logarithmic coordinates, and the target WS spectrum power shows a trend of increasing and then decreasing, with the highest not exceeding 10^3. In a comprehensive view, in the TT vibration suppression is mainly from the suppression of the top of the tower, and the TT needs to choose a suitable height to reduce the dynamic displacement. At the same time, in the area with many typhoons, the design safety factor of conductors and ground wires should be increased as much as possible to avoid the damage of transmission lines caused by typhoons. However, the finite element model constructed by the study does not achieve dynamic similarity, so subsequent optimisation is needed.

Data Availability Statement

The datasets used and/or analysed during the current study are available from the corresponding author on reasonable request.

Conflicts of Interest

The authors declared that this article is free of conflict of interest.

Funding Statement

References

[1] K. Jain and A. Saxena, Simulation on supplier side bidding strategy at day-ahead electricity market using ant lion optimizer, *Journal of Computational and Cognitive Engineering*, *2*(1), 2023, 17–27.

[2] Y. Tang and Y. Huang, Research on construction technology of deep foundation pit of high voltage transmission line in plateau area, *Academic Journal of Science and Technology*, *4*(2), 2022, 112–115.

[3] X. Song, Y. Chen, C. Bo, and J. Wu, Response control of a transmission tower-line system under wind excitations by electromagnetic inertial mass dampers, *Advances in Structural Engineering*, *25*(16), 2022, 3334–3348.

[4] A.B. Jeddi, A. Shafieezadeh, J. Hur, J.G. Ha, D. Hahm, and M.K. Kim, Multi-hazard typhoon and earthquake collapse fragility models for transmission towers: An active learning reliability approach using gradient boosting classifiers, *Earthquake Engineering and Structural Dynamics*, *51*(15), 2022, 3552–3573.

[5] H. Zuo and H. Guo, Nonlinear damage identification method of transmission tower structure based on general expression for linear and nonlinear autoregressive model and Itakura distance, *Structural Health Monitoring*, *22*(1), 2023, 19–38.

[6] P.Y. Kong and Y. Song, Artificial-neural-network-assisted sensor clustering for robust communication network in IoT-based electricity transmission line monitoring, *IEEE Internet of Things Journal*, *9*(17), 2022, 16701–16713.

[7] M.R.M. Asyraf, M.R. Ishak, A. Syamsir, A.L. Amir, N.M. Nurazzi, M.N.F. Norrrahim, and M.R. Razman, Filament-wound glass-fibre reinforced polymer composites: Potential applications for cross arm structure in transmission towers, *Polymer Bulletin*, *80*(2), 2023, 1059–1084.

[8] J.A. Bennett, C.N. Trevisan, J.F. DeCarolis, C. Ortiz-García, M. Pérez-Lugo, B.T. Etienne, and A.F. Clarens, Extending energy system modelling to include extreme weather risks and application to hurricane events in Puerto Rico, *Nature Energy*, *6*(3), 2021, 240–249.

[9] Ü.K. İşleyen, R. Ghoroubi, Ö. Mercimek, Ö. Anil, and R.T. Erdem, Behavior of glulam timber beam strengthened with carbon fiber reinforced polymer strip for flexural loading, *Journal of Reinforced Plastics and Composites*, *40*(17–18), 2021, 665–685.

[10] B. Zhao, D. Wu, and Z. Lu, Shaking table test and numerical simulation of the vibration control performance of a tuned mass damper on a transmission tower, *Structure and Infrastructure Engineering*, *17*(8), 2021, 1110–1124.

[11] T.H. Nguyen and A.T. Vu, Weight optimization of steel lattice transmission towers based on Differential Evolution and machine learning classification technique, *Frattura ed Integrità Strutturale*, *16*(59), 2022, 172–187.

[12] V.E. Ogbonna, A.P.I. Popoola, O.M. Popoola, and S.O. Adeosun, A review on corrosion, mechanical, and electrical properties of glass fiber-reinforced epoxy composites for high-voltage insulator core rod applications: Challenges and recommendations, *Polymer Bulletin*, *79*(9), 2022, 6857–6884.

[13] E. Tapia-Hernández and D. De-León-Escobedo, Vulnerability of transmission towers under intense wind loads, *Structure and Infrastructure Engineering*, *18*(9), 2022, 1235–1250.

[14] Z. Qiu, X. Zhu, C. Liao, D. Shi, Y. Kuang, Y. Li, and Y. Zhang, Detection of bird species related to transmission line faults based on lightweight convolutional neural network, *IET Generation, Transmission and Distribution*, *16*(5), 2022, 869–881.

[15] X. Lei, D.M. Siringoringo, Z. Sun, and Y. Fujino, Displacement response estimation of a cable-stayed bridge subjected to various loading conditions with one-dimensional residual convolutional autoencoder method, *Structural Health Monitoring*, *22*(3), 2023, 1790–1806.

[16] W. Wang, K. Chen, Y. Bai, Y. Chen, and J. Wang, New estimation method of wind power density with three-parameter Weibull distribution: A case on Central Inner Mongolia suburbs, *Wind Energy*, *25*(2), 2022, 368–386.

[17] M. Puccioni and G.V. Iungo, Spectral correction of turbulent energy damping on wind lidar measurements due to spatial

averaging, *Atmospheric Measurement Techniques*, *14*(2), 2021, 1457–1474.

[18] Q. Zhang, J. He, Y. Xu, Z. Hong, Y. Chen, and K. Strunz, Average-value modelling of direct-driven PMSG-based wind energy conversion systems, *IEEE Transactions on Energy Conversion*, *37*(1), 2021, 264–273.

Biographies

Zhengfa Li received the degree in power electronics and power transmission engineering from Lanzhou University of Technology in 2016. Currently, he works as the Technology Director with the State Grid Gansu Electric Power Company Construction Branch. His research interest is in technical management of transmission and transformation engineering construction.

Jianwei Zhang received the degree in electrical engineering from Xi'an Jiaotong University in 2011. Currently, he works as the Vice-Director with the State Grid Gansu Electric Power Company Construction Branch. His research interest is in engineering construction management.

Haining Wang received the degree in thermal power engineering from Changsha University of Science & Technology in 2000. Currently, he works as the Project Manager with the State Grid Gansu Electric Power Company Construction Branch. His research interest is in engineering construction management.
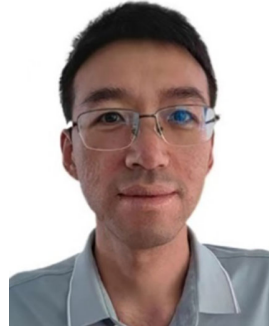
Yijun Bao received the degree in architecture and civil engineering from Lanzhou Jiaotong University in 2016. Currently, he works as the Technology Director with the State Grid Gansu Electric Power Company Construction Branch. His research interest is in engineering construction management and technology and economy management.